

---

# eXplaining to Learn (eX2L): Regularization Using Contrastive Visual Explanation Pairs for Distribution Shifts

---

Paulo Mario P. Medina<sup>1</sup> Jose Marie Antonio Miñoza<sup>1</sup> Sebastian C. Ibañez<sup>1</sup>

## Abstract

Despite extensive research into mitigating distribution shifts, many existing algorithms yield inconsistent performance, often failing to outperform baseline Empirical Risk Minimization (ERM) across diverse scenarios. Furthermore, high algorithmic complexity frequently limits interpretability and offers only an indirect means of addressing spurious correlations. We propose eXplaining to Learn (eX2L): an interpretable, explanation-based framework that decorrelates confounding features from a classifier’s latent representations during training. eX2L achieves this by penalizing the similarity between Grad-CAM activation maps generated by a primary label classifier and those from a concurrently trained confounder classifier. On the rigorous *Spawrious Many-to-Many Hard Challenge* benchmark, eX2L achieves an average accuracy (AA) of  $82.24\% \pm 3.87\%$  and a worst-group accuracy (WGA) of  $66.31\% \pm 8.73\%$ , outperforming the current state-of-the-art (SOTA) by 5.49% and 10.90%, respectively. Beyond its competitive performance, eX2L demonstrates that functional domain invariance can be achieved by explicitly decoupling label and nuisance attributes at the group level.

## 1. Introduction

Standard machine learning models rely on the assumption that training and test data are independently and identically distributed (i.i.d.) (Ye et al., 2021). When this assumption is violated, models often fail to generalize, instead relying on spurious correlations, statistical patterns in the training data that are not conceptually predictive of the actual labels (Monga et al., 2025; Suhail et al., 2025; Koh et al., 2020). These violations typically manifest as two types of distribution shifts: subpopulation shifts and domain generalization.

<sup>1</sup>Center for AI Research PH. Correspondence to: Paulo Mario P. Medina.

Subpopulation shifts occur when the proportions of demographic or contextual variables change between training and deployment (Koh et al., 2020; Yang et al., 2023). Consider a medical diagnostic tool trained on radiographs: if the training set is 80% White and 20% other ethnicities, but the model is deployed in an Asian country where the population is 90% Asian and 10% White/other, the model may suffer from catastrophic performance degradation due to its initial bias toward White physiological features.

In contrast, domain generalization involves learning from one or more “source domains” to perform on entirely unseen “target domains” at deployment (Koh et al., 2020; Ye et al., 2021). For instance, a model trained on Malaysian wildlife images may struggle to classify animals in Philippine wildlife images due to differing camera qualities, lighting, or background vegetation. In these cases, the model often “cheats” by learning the background rather than the animal itself.

While various loss-level regularization methods exist, they face three primary hurdles:

1. **Blind Regularization:** Many black-box algorithms do not explicitly target the spurious correlations causing the performance drop (Wiles et al., 2022).
2. **Inconsistent Performance:** No single algorithm consistently outperforms Empirical Risk Minimization (ERM) across all datasets, reflecting the “no-free-lunch” theorem in machine learning (Wiles et al., 2022; Gulrajani & Lopez-Paz, 2021).
3. **Lack of Interpretability:** Technically sophisticated methods, such as Domain-Adversarial Neural Networks (DANN) (Ganin et al., 2016), rely on mechanisms like gradient reversal that are difficult to explain to non-technical stakeholders, hindering trust in sensitive deployments.

We therefore ask: *can penalizing the spatial overlap of gradient-based explanations from a label and confounder classifier serve as a direct, interpretable regularizer for distribution shift robustness, without sacrificing predictive accuracy?*

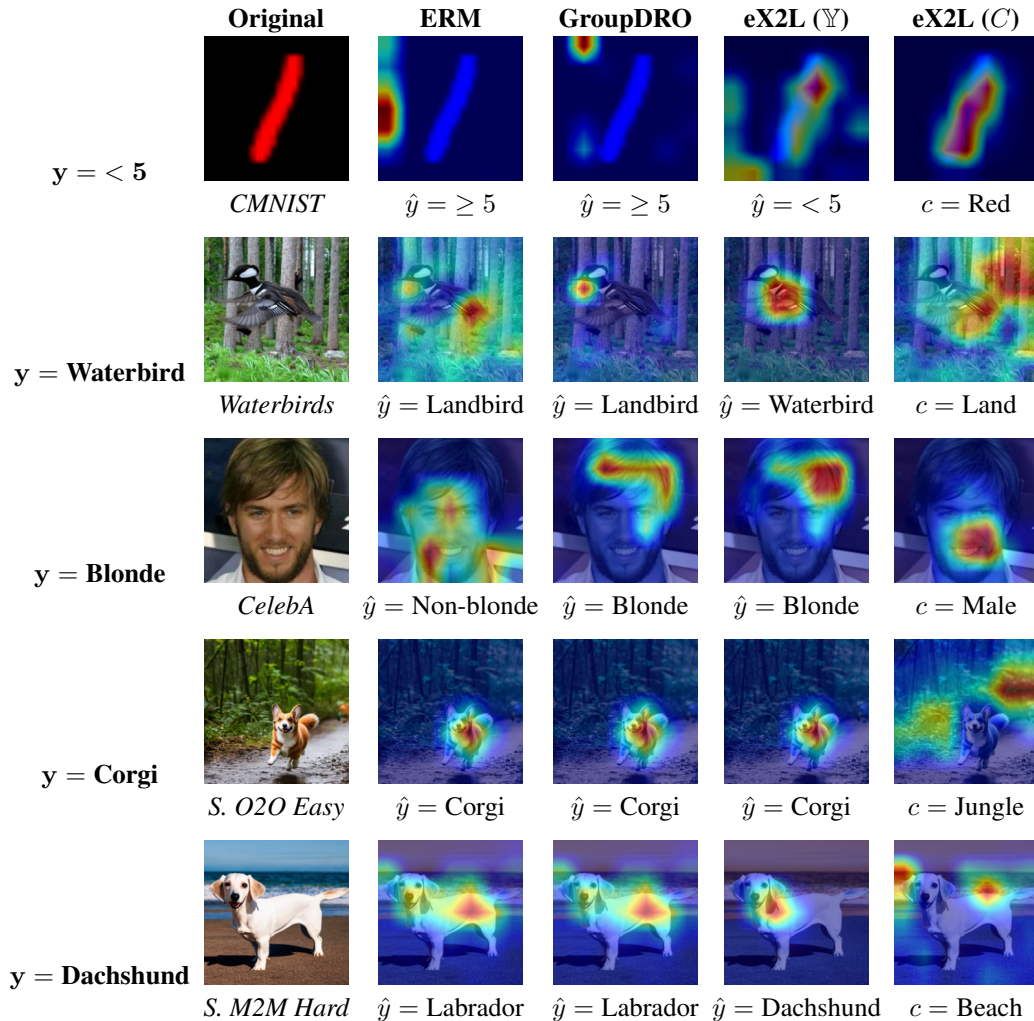


Figure 1. Grad-CAM plots of eX2L and others with their corresponding true labels  $y$ , predicted labels  $\hat{y}$ , and true confounders  $c$ . eX2L’s 11.91% improvement in worst-group accuracy against GroupDRO can be directly attributed to the mechanical shift visualized in the last row where GroupDRO’s and ERM’s attention is diffused across the background: eX2L restricts focus exclusively to the dog’s ear, effectively ignoring the confounding beach texture.

To bridge these gaps, we introduce eXplaining to Learn (eX2L), a framework at the intersection of OOD generalization and XAI. eX2L regularizes training by penalizing the spatial overlap between the Grad-CAM explanations of a label classifier and a concurrently trained confounder model. By forcing the primary model to diverge from the confounder’s visual focus, eX2L explicitly decouples spurious correlations and promotes domain invariance. Critically, our results demonstrate that interpretability can act as a *catalyst* for predictive robustness rather than a trade-off against it, challenging the prevailing assumption that more explainable models are necessarily less accurate.

## 2. Related Works

**Subpopulation Shifts and Spurious Correlations** While domain generalization dominates the literature, subpopulation shift has emerged as a distinct challenge where models rely on spurious correlations, non-predictive features that correlate with labels in specific groups (Koh et al., 2020; Yang et al., 2023). Current state-of-the-art (SOTA) loss-level regularization, such as GroupDRO, employs minimax fairness to minimize worst-group risk (Sagawa et al., 2020). However, optimizing for the worst-case group often comes at the expense of overall average performance and only indirectly addresses the underlying spurious attributes (Shen & Zhao, 2025).

Other approaches which also require group-level annotations like Just Train Twice (JTT) and Deep Feature

Reweighting (DFR) address these shifts via data-centric two-step pipelines involving initial training and subsequent fine-tuning on curated subsets (Liu et al., 2021a; Kirichenko et al., 2023). Given the fundamental difference in methodology, this study focuses on comparing eX2L against loss-based regularization methods, which offer more streamlined, single-stage training.

**Domain Generalization** Standard DG approaches prioritize domain invariance, attempting to minimize the divergence between the empirical loss of available domains and the theoretical loss of the global distribution (Liu et al., 2021b; Ye et al., 2021). Despite these theoretical foundations, many DG algorithms fail to consistently outperform Empirical Risk Minimization (ERM) on most image datasets (Gulrajani & Lopez-Paz, 2021).

Recent perspectives suggest decomposing the label space into label and nuisance attributes (Wiles et al., 2022). Under this framework, distribution shift is viewed as a problematic correlation between labels and nuisances in the source domain. eX2L builds on this motivation by explicitly decoupling these attributes through explanation-based learning.

**Explanation-based Learning** Existing explanation-based learning utilizes adversarial or contrastive training to align robust and non-robust representations (Han & Tsvetkov, 2021; Dammu & Shah, 2023). For example, Hagos et al. (2022) used Grad-CAM maps alongside expensive ground-truth masks to reduce spurious reliance, while Dammu & Shah (2023) used several local surrogate models per class and compared their Grad-CAM maps with the primary classifier’s Grad-CAM maps, only to detect spurious visual attributes. However, eX2L departs from these works in two significant ways:

1. It requires only two concurrent classifiers (label and confounder), and it does not require ground-truth annotation masks, only confounder labels.
2. It utilizes Grad-CAM pairs not just for detection, but to automate the debiasing process, directly improving downstream performance without requiring manual annotation masks.

### 3. Proposed Method

#### 3.1. Problem Setting

We define a training set of images  $\mathcal{X}$ , labels  $\mathcal{Y}$ , and *a priori* confounding variables  $C$ . Following the group-based framework of Sagawa et al. (2020), each input  $\mathbf{x} \in \mathcal{X}$  belongs to a group  $g$  defined by the cross-product of labels and confounders:  $g \in C \times \mathcal{Y}$ .

For the primary classification task, we define a latent representation function  $h_y : \mathbf{x} \rightarrow Z$  and a classifier  $f_y : Z \rightarrow \mathcal{Y}$ . Following Ming et al. (2022), we assume that in the presence of distribution shifts the latent representation  $Z$  admits the decomposition:

$$Z = Z_{\text{inv}} + Z_{\text{spu}} \quad (1)$$

where  $Z_{\text{inv}}$  represents invariant features (conceptually predictive of labels) and  $Z_{\text{spu}}$  represents spurious/confounding features (predictive of the group  $g$  but not the label  $\mathcal{Y}$ ). Because  $P(Z_{\text{spu}}|\mathcal{X}_{\text{train}})$  differs significantly from  $P(Z_{\text{spu}}|\mathcal{X}_{\text{test}})$ , the model’s reliance on  $Z_{\text{spu}}$  leads to performance degradation at deployment (Ming et al., 2022).

To isolate and remove  $Z_{\text{spu}}$ , we introduce a secondary confounder model  $(h_c, f_c)$  trained to predict the confounder labels  $C$ . While a direct penalty on the similarity of representations  $Z$  and  $Z_c$  might seem intuitive, such an approach is not spatially target-specific. It may penalize relevant features rather than specific confounding regions.

#### 3.2. The eX2L Algorithm

To ensure the penalty is target-specific, we utilize Grad-CAM (Selvaraju et al., 2019), chosen over input-gradient methods (e.g., SHAP, Integrated Gradients) for its faithfulness to model reparametrization rather than input structure (Adebayo et al., 2018) (see Appendix B). For a target class  $t$ , the importance weight  $\alpha_k^t$  for the  $k$ -th activation map  $A^k$  is acquired through a global average pooling of the target logit’s gradients with respect to each map’s pixel:

$$\alpha_k^t = \frac{1}{P} \sum_i \sum_j \frac{\partial \hat{t}^t}{\partial A_{i,j}^k} \quad (2)$$

where  $P$  is the total number of pixels in the map.

The heatmap,  $L_{\text{Grad-CAM}}^t = \text{sg}(\text{ReLU}(\sum_k \alpha_k^t A^k))$ , where  $\text{sg}(\cdot)$  denotes the stop-gradient operator that treats its argument as a constant during backpropagation, highlights the regions the model prioritizes (Selvaraju et al., 2019). Detaching the heatmap avoids the computational cost of second-order derivatives and treats the visual explanation as a static spatial prior, allowing eX2L to minimize the spatial overlap between the label and confounder model explanations.

If the label model and the confounder model rely on the same pixels, the label model is likely operating by *shortcut learning* using spurious background cues. Forcing their heatmaps to be spatially disjoint compels the label model to identify its own unique, invariant features. Using the heatmaps for the label and confounder, we define the similarity loss  $l_{\text{sim}}$  as:

$$\mathcal{L}_{\text{sim}} = S(L_{\text{Grad-CAM}}^y, L_{\text{Grad-CAM}}^c) \quad (3)$$

where  $S$  is a similarity metric (e.g., Cosine Similarity or Mean Squared Error). The total eX2L training objective  $\hat{R}_{\text{eX2L}}$  is formulated as:

$$\hat{R}_{\text{eX2L}}(\theta, \phi) = \mathbb{E}_{(\mathbf{x}, y, c) \sim D_{\text{train}}} [\mathcal{L}(\mathbf{x}, y; \theta) + \lambda_c \mathcal{L}(\mathbf{x}, c; \phi) + \lambda_{\text{sim}} \mathcal{L}_{\text{sim}}(\mathbf{x}, y, c; \theta, \phi)] \quad (4)$$

where  $\theta$  refers to the label model’s parameters,  $\phi$  refers to the confounder model’s parameters,  $\lambda_c$  refers to the confounder model hyperparameter, and the  $\lambda_{\text{sim}}$  refers to the similarity loss hyperparameter.

### 3.3. Optimization and Sampling

We define *functional domain invariance* as the property of a learned representation whose distribution is invariant across environments, even when the model is trained without environment labels or adversarial objectives. As shown in Section 5, eX2L achieves this as an emergent property of the Grad-CAM similarity penalty.

The objective is to find the parameters  $\theta^*$  that maximize the mean of the Worst-Group Accuracy (WGA) and Average Accuracy (AA) at test time:

$$WGA = \min_g \mathbb{E}_{(\mathbf{x}, y) \sim D_{\text{test}}^g} [\mathbf{1}_{\hat{y}_\theta = y}] \quad (5)$$

$$AA = \mathbb{E}_{(\mathbf{x}, y) \sim D_{\text{test}}} [\mathbf{1}_{\hat{y}_\theta = y}] \quad (6)$$

$$\theta^* = \arg \max_{\theta \in \Theta} \frac{WGA(\theta) + AA(\theta)}{2} \quad (7)$$

Note that  $\theta^*$  defines the *model selection criterion* used for checkpointing, not the training objective itself; the model is trained via  $\hat{R}_{\text{eX2L}}$ , while  $\theta^*$  selects the checkpoint that best balances WGA and AA. To optimize this, we contrast two sampling strategies:

- **Random Sampling:** Follows the prevailing training distribution.
- **Uniform Group Sampling:** Samples  $(\mathbf{x}, y, c)$  uniformly across all non-empty groups  $g$ .

Uniform Group Sampling is found to be critical for eX2L (See Appendix A), as it prevents the model from learning the inherent label-confounder proportions as a shortcut, further forcing the algorithm to rely on the Grad-CAM penalty to distinguish between invariant and spurious features.

Furthermore, we distinguish these from **Uniform Environment Sampling**, a method typically used in domain generalization to sample uniformly from predefined environments.

---

### Algorithm 1 eXplaining to Learn (eX2L)

---

**Input:** Training set  $\mathcal{D}$ , label model  $m_\theta$ , confounder model  $m_\phi$ , loss functions  $\mathcal{L}$ , similarity metric  $S$ , hyperparameters  $\lambda_c, \lambda_{\text{sim}}$ .

**Initialize:** Weights  $\theta, \phi$  and optimizers.

**for** each epoch **do**

**for** batch  $(\mathbf{x}, y, c) \in \mathcal{D}$  **do**

    // Forward Pass

    Pass  $\mathbf{x}$  through models to get latent  $z$  and logits:

$\mathbf{s}_y \leftarrow m_\theta(\mathbf{x}), \mathbf{s}_c \leftarrow m_\phi(\mathbf{x})$

    // Targeted Logit Selection

    Select target-class scores:  $\hat{s}_y \leftarrow \mathbf{s}_y[y]$

    and  $\hat{s}_c \leftarrow \mathbf{s}_c[c]$

    // Grad-CAM Heatmap Generation

    Extract feature maps  $A_y, A_c$  from target layers.

**for**  $k \in \{1, \dots, |A_y|\}$  **do**

$$\alpha_k^y \leftarrow \frac{1}{P} \sum_i \sum_j \frac{\partial \hat{y}^y}{\partial A_{y,i,j}^k}$$

$$\alpha_k^c \leftarrow \frac{1}{P} \sum_i \sum_j \frac{\partial \hat{c}^c}{\partial A_{c,i,j}^k}$$

**end for**

    // Heatmap Detachment

$$L_{\text{Grad-CAM}}^y \leftarrow \text{sg}(\text{ReLU}(\sum_k \alpha_k^y \cdot A_y^k))$$

$$L_{\text{Grad-CAM}}^c \leftarrow \text{sg}(\text{ReLU}(\sum_k \alpha_k^c \cdot A_c^k))$$

    // Objective Function

$$\mathcal{L}_{\text{task}} \leftarrow \mathcal{L}(\mathbf{s}_y, y) + \lambda_c \mathcal{L}(\mathbf{s}_c, c)$$

    // Similarity of Detached Grad-CAM Heatmaps

$$\mathcal{L}_{\text{sim}} \leftarrow S(L_{\text{Grad-CAM}}^y, L_{\text{Grad-CAM}}^c)$$

$$\mathcal{L}_{\text{total}} \leftarrow \mathcal{L}_{\text{task}} + \lambda_{\text{sim}} \mathcal{L}_{\text{sim}}$$

    // Optimization

    Update  $\theta, \phi$  via  $\nabla_{\theta, \phi} \mathcal{L}_{\text{total}}$

**end for**

**end for**

---

We do not employ environment-based sampling as  $\hat{R}_{\text{eX2L}}$  is specifically designed for the group-based setting, focusing more on the label and confounder intersection of attributes. The complete training procedure is summarized in Algorithm 1.

### 3.4. Theoretical Motivation

The design of eX2L is grounded in three key observations from the explainability and representation learning literature.

**Grad-CAM as a Faithful Localization Mechanism.** Crucially, Adebayo et al. (2018) demonstrated that unlike backpropagation-based attribution methods, which remain largely invariant to network reparameterization and behave similarly to edge detectors, gradient-based methods like Grad-CAM produce *target-specific* attributions that faithfully reflect the model’s learned parameters. This property makes Grad-CAM well-suited for identifying which spa-

tial regions drive predictions for both the label  $y$  and the confounder  $c$  throughout training.

**Disjoint Attention Induces Feature Decorrelation.** Let  $\mathcal{A}_y \subseteq \mathcal{I}$  and  $\mathcal{A}_c \subseteq \mathcal{I}$  denote the spatial regions attended to by the label and confounder models, respectively, where  $\mathcal{I}$  represents the image domain. By minimizing the similarity  $S(L_{\text{Grad-CAM}}^y, L_{\text{Grad-CAM}}^c)$ , we encourage  $|\mathcal{A}_y \cap \mathcal{A}_c|$  to be small. This spatial disjointness discourages the label classifier from relying on confounding regions, effectively forcing it to discover alternative features that are predictive of  $y$  but not of  $c$ .

This mechanism can be viewed as inducing a form of *functional disentanglement*: rather than requiring full statistical independence of latent factors, which is provably difficult without inductive biases (Locatello et al., 2019), eX2L leverages explicit confounder supervision to achieve a weaker but practically sufficient objective where the label prediction  $f_y$  becomes invariant to the spatial support of the confounder.

**Connection to Information-Theoretic Principles.** The information bottleneck principle (Tishby & Zaslavsky, 2015) posits that an optimal representation  $Z$  should maximize information about the target  $Y$  while minimizing information about the input  $X$  that is irrelevant to  $Y$ .

While we do not directly optimize an information-theoretic objective, the geometric constraint on Grad-CAM overlap serves as a computationally tractable proxy. By enforcing spatial disjointness between label and confounder attention maps, eX2L acts as a regularizer that reduces the model’s capacity to exploit confounding features and encourages the model to rely on invariant features that generalize across groups.

## 4. Experimental Setup

### 4.1. Datasets and Benchmarks

We evaluate eX2L across two primary challenges: subpopulation shifts and domain generalization.

**Subpopulation Shifts** We utilize standard benchmarks including *CMNIST* (Arjovsky et al., 2019), *Waterbirds*, and *CelebA* (Sagawa et al., 2020). These datasets allow us to test eX2L on synthetic subject-inherent correlations (e.g., color in CMNIST), natural background correlations (e.g., land/water in Waterbirds), and real-world attribute correlations (e.g., gender in CelebA).

**Domain Generalization** We employ the *Spawrious* benchmark (Lynch et al., 2025), specifically the *One-to-One Easy* and *Many-to-Many Hard* challenges. These tasks evaluate eX2L’s ability to generalize across shifting back-

ground confounders (e.g., Dirt  $\rightarrow$  Beach vs. Dirt, Snow  $\rightarrow$  Beach, Jungle). For Spawrious, the confounder labels  $C$  correspond to the background category provided by the dataset (Lynch et al., 2025), and groups  $g$  are defined as the cross-product of dog breed label and background confounder, enabling the group-based eX2L setup to apply directly.

### 4.2. Model Architecture

All experiments utilize a **ResNet-50** backbone initialized with IMAGENET1K\_V2 weights. To generate Grad-CAM maps, we use the final convolutional block of the module, as it captures semantically rich features more effectively than initial layers (Selvaraju et al., 2019). These heatmaps are then detached before backpropagation.

### 4.3. Baselines

We compare eX2L against Empirical Risk Minimization (ERM) as a general baseline. For subpopulation shifts, we use **GroupDRO** (Sagawa et al., 2020). For domain generalization, we compare against SOTA environment-based methods including **IRM**, **MMD**, **CORAL**, **DANN**, and **CDAN**. We prioritize regularization-based methods, over data augmentation and fine-tuning methods, to ensure an analogous comparison to the eX2L framework.

### 4.4. eX2L Regularization and Strategy

We initially screened 11 similarity functions under two sampling regimes (random and uniform group sampling), totaling 22 configurations. To prioritize robustness, the top three unique setups, measured by Worst-Group Accuracy (WGA) on CMNIST and Waterbirds, were selected for full evaluation. The final functions include: *Negative MAE*, *Negative Jensen-Shannon distance*, *Cosine Similarity*, *SSIM*, and *Soft Dice*.

### 4.5. Implementation Details

**Data Generation** We extended the DomainBed (Gulrajani & Lopez-Paz, 2021) repository to explicitly retrieve confounder annotations for *CMNIST* and *Spawrious*. We modified the WILDS repository (Koh et al., 2020) such as *Waterbirds* and *CelebA* to simulate subpopulation shifts by creating varied group proportions across environments.

**Training Strategy** Models were trained using SGD with a batch size of 128. Hyperparameters were tuned via randomized search (20 trials) following the distributions in Gulrajani & Lopez-Paz (2021). For eX2L-specific parameters ( $\lambda_c$  and  $\lambda_{sim}$ ), distribution bounds were determined via an initial grid search. We employed early stopping (patience = 10; min\_delta =  $10^{-3}$ ) based on the mean of Average Accuracy (AA) and WGA.

Table 1. CMNIST and Waterbirds Experiment Results

Algorithms		Subpopulation Shift			
Name	Sampling	CMNIST		Waterbirds	
		AA	WGA	AA	WGA
<i>Baselines</i>					
ERM	Random	32.96 ±2.9%	25.11 ±2.5%	62.86 ±15.8%	23.68 ±21.1%
IRM	Uniform Env.	65.11 ±1.1%	64.59 ±0.9%	89.16 ±2.4%	84.42 ±3.0%
MMD	Uniform Env.	65.41 ±0.8%	61.98 ±1.4%	90.81 ±1.1%	85.64 ±0.2%
CORAL	Uniform Env.	63.62 ±4.1%	59.23 ±7.0%	90.00 ±0.8%	85.41 ±0.8%
DANN	Uniform Env.	67.32 ±1.6%	66.42 ±1.6%	90.71 ±0.6%	85.41 ±0.8%
CDAN	Uniform Env.	35.25 ±24.4%	21.00 ±18.8%	89.57 ±1.7%	84.71 ±1.8%
GroupDRO	Uniform Group	66.14 ±2.1%	63.79 ±3.5%	90.50 ±0.4%	85.95 ±1.2%
<i>Ours</i>					
<b>eX2L-MAE</b>	<b>Uniform Group</b>	<b>69.02 ±0.5%</b>	<b>67.63 ±1.4%</b>	89.59 ±0.5%	<b>87.45 ±0.6%</b>
eX2L-Cosine	Uniform Group	67.90 ±0.6%	66.15 ±1.0%	90.85 ±1.0%	85.72 ±0.7%
<b>eX2L-Soft Dice</b>	<b>Uniform Group</b>	<b>66.75 ±1.6%</b>	<b>65.14 ±2.1%</b>	<b>92.12 ±0.7%</b>	<b>86.92 ±0.6%</b>
<b>eX2L-JS Dist.</b>	<b>Uniform Group</b>	<b>69.66 ±0.9%</b>	<b>66.88 ±2.3%</b>	89.18 ±1.9%	85.10 ±2.3%
eX2L-SSIM	Uniform Group	67.85 ±1.0%	65.87 ±2.1%	89.77 ±1.5%	85.10 ±1.2%

Table 2. Spawrious Experiment Results

Algorithms		Domain Generalization			
Name	Sampling	Spawrious O2O (Easy)		Spawrious M2M (Hard)	
		AA	WGA	AA	WGA
<i>Baselines</i>					
ERM	Random	91.00 ±1.1%	84.12 ±2.0%	77.37 ±2.4%	54.91 ±2.5%
IRM	Uniform Env.	93.01 ±1.3%	86.20 ±3.1%	64.66 ±0.5%	35.19 ±2.3%
MMD	Uniform Env.	93.13 ±1.5%	86.17 ±2.9%	76.64 ±3.9%	54.35 ±4.7%
CORAL	Uniform Env.	93.14 ±1.6%	86.43 ±3.0%	76.74 ±3.5%	53.74 ±4.7%
DANN	Uniform Env.	94.04 ±1.0%	87.55 ±1.2%	76.75 ±4.8%	55.41 ±9.3%
CDAN	Uniform Env.	93.43 ±1.7%	85.24 ±2.9%	73.95 ±9.3%	48.23 ±12.4%
<b>GroupDRO</b>	<b>Uniform Group</b>	<b>95.13 ±0.3%</b>	<b>90.32 ±1.0%</b>	77.70 ±2.2%	54.40 ±1.4%
<i>Ours</i>					
<b>eX2L-MAE</b>	<b>Uniform Group</b>	<b>94.30 ±1.0%</b>	<b>88.05 ±1.1%</b>	<b>82.24 ±3.9%</b>	<b>66.31 ±8.7%</b>
eX2L-Cosine	Uniform Group	93.97 ±0.3%	87.71 ±1.0%	81.37 ±7.5%	64.25 ±13.3%
eX2L-Soft Dice	Uniform Group	91.34 ±1.2%	81.78 ±2.1%	76.10 ±4.5%	54.09 ±7.8%
eX2L-JS Dist.	Uniform Group	93.81 ±1.2%	87.74 ±2.5%	60.77 ±24.1%	38.02 ±36.1%
eX2L-SSIM	Uniform Group	93.52 ±1.0%	85.96 ±2.4%	74.16 ±6.6%	46.10 ±11.9%

#### 4.6. Evaluation Criteria

We report the mean and standard deviation across three runs using different seeds (42, 8, 777). Following Sagawa et al. (2020), we use **Average Accuracy (AA)** and **Worst-Group Accuracy (WGA)** to evaluate the performance trade-offs inherent in distribution shifts.

#### 4.7. Auxiliary Studies

Beyond performance metrics, we conduct the following analyses:

- **Visual Interpretability:** Visualizing feature attribution via Grad-CAM (Selvaraju et al., 2019).

- **Latent Representation:** Qualitative latent space evaluation via UMAP (McInnes et al., 2018) and quantitative distribution shift measurement via linear MMD (Gretton et al., 2012).

- **Efficiency:** Analyzing the training time vs. performance trade-off in complex settings using the *Hard Spawrious* benchmark.

Refer to Appendix B for additional details regarding the experimental setup.

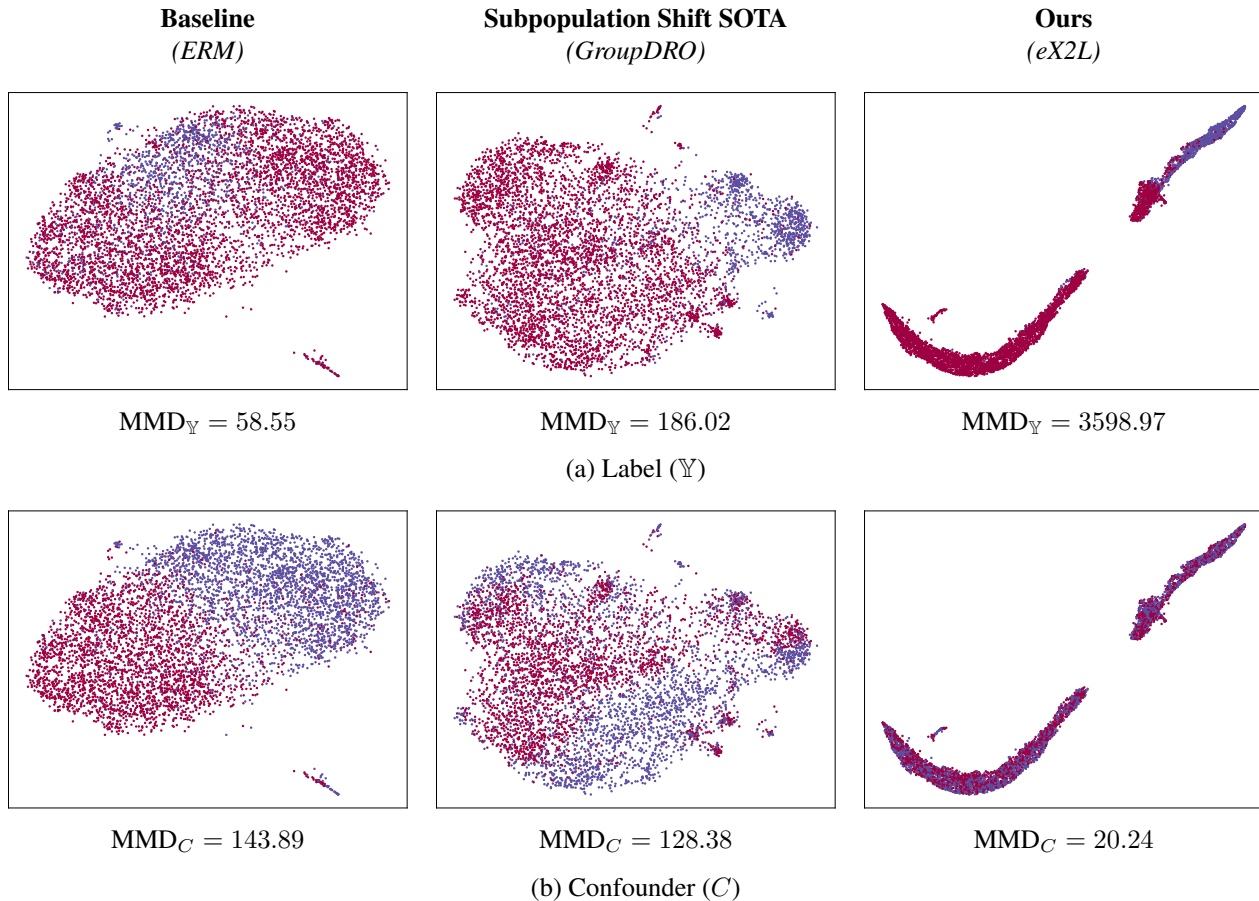


Figure 2. UMAP Plots of different algorithms’ latent representations on the *Waterbirds* dataset. (a) maps the color of each point by the label while (b) maps the color of each point by the confounder. The compactness, clear label separation, and lack of confounder reliance of the representations supports the observed targeted visual focus by eX2L as seen in Figure 1

## 5. Results and Discussion

### 5.1. Experiment Results

**Subpopulation Shift (Table 1)** eX2L-based algorithms consistently outperform SOTA baselines in mitigating subpopulation shifts:

- **eX2L-MAE Dominance:** eX2L-MAE achieves the highest WGA on *CMNIST* (67.63%) and competitive results on *Waterbirds*, maintaining lower variance compared to baselines like CDAN.
- **Metric Sensitivity:** While eX2L-JS Dist. and eX2L-Soft Dice prioritize AA, eX2L-MAE is more effective for WGA. This suggests that MAE’s stringent pixel-to-pixel penalty better prevents the model from latching onto spurious features.

**Domain Generalization (Table 2)** The *Spawrious* results highlight a distinct bias-variance trade-off:

- **Task Complexity:** While GroupDRO excels in the *Easy (O2O)* setting, eX2L-MAE is the only algorithm to surpass 80% AA and 60% WGA in the *Hard (M2M)* benchmark.
- **Performance Gains:** In the *Hard* setting, eX2L-MAE outperforms DANN, the strongest domain generalization baseline, by 5.49% in AA and 10.90% in WGA, and surpasses GroupDRO, the strongest overall baseline for AA (77.70%), by 4.54% in AA.
- **Robustness:** eX2L is uniquely robust to “many-to-many” correlations where multiple unseen backgrounds are present at test time, making it better suited for complex, real-world distribution shifts than existing regularization methods.

On *CelebA*, eX2L-Cosine achieves 84.07% WGA, matching GroupDRO’s best WGA while maintaining 91.19% AA; hair color’s diffuse geometry favors softer metrics over pixel-wise penalties (see Appendix C and Appendix F).

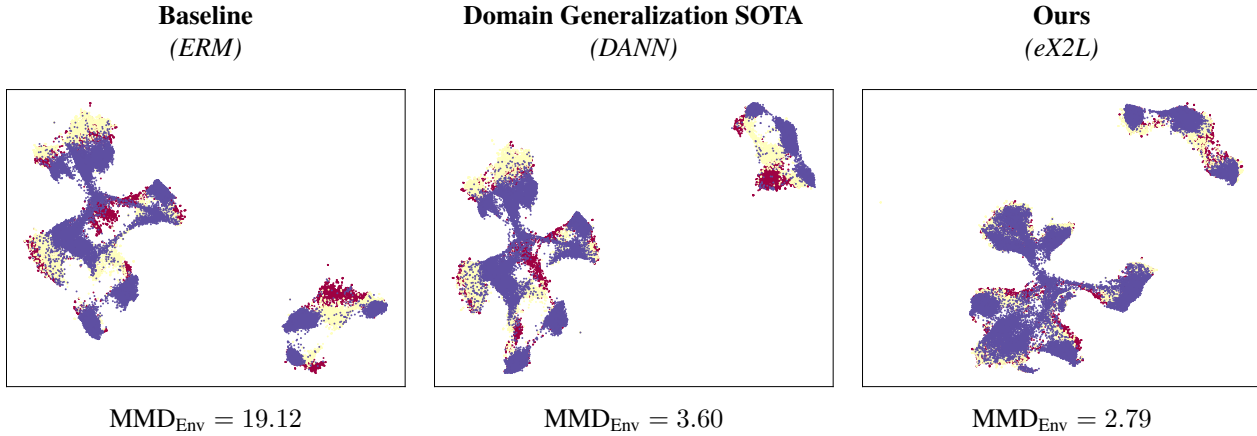


Figure 3. UMAP Plots of different algorithms’ latent representations on the *Hard Many-to-Many Spawrious* dataset. Colors map the three defined training and test environments. While not explicitly using environmental annotations, eX2L demonstrates better domain invariance than DANN, as evidenced by its lower  $MMD_{Env}$  and more highly interspersed environments.

### 5.2. Visual Interpretability Analysis

Based on Figure 1, Grad-CAM heatmaps confirm that eX2L’s gains stem from a conceptual shift in feature attribution:

- **Structural Anchoring:** eX2L focuses on semantically invariant regions (e.g., digit edges for *CMNIST*, ears for *Dachshunds*), while baselines diffuse attention across spurious background cues.

### 5.3. Latent Representation Analysis

**Subpopulation Shift (Figure 2)** The UMAP visualizations of the *Waterbirds* dataset demonstrate that eX2L achieves superior feature disentanglement compared to SOTA baselines:

- **Label Separation:** While ERM and GroupDRO exhibit overlapping or dispersed clusters, eX2L produces compact, well-separated representations with an exceptionally high  $MMD_{\mathcal{Y}}$  (3598.97), indicating a highly precise decision boundary.
- **Confounder Independence:** Unlike ERM, which shows distinct confounder clusters (high  $MMD_C$ ), eX2L achieves near-total interspersion of confounder features ( $MMD_C = 20.24$ ). This proves the model has successfully discarded spurious confounder signals in favor of class-relevant features.

**Domain Generalization (Figure 3)** The latent space on the *Hard M2M Spawrious* dataset highlights the emergence of *functional domain invariance*:

- **Environmental Invariance:** eX2L exhibits the highest degree of environment interspersing, yielding the

lowest  $MMD_{Env}$  (2.79). Remarkably, this surpasses DANN (3.60), the domain generalization SOTA explicitly designed for this task.

- **Intrinsic Alignment:** eX2L aligns training and test distributions without requiring environmental labels or adversarial objectives.

### 5.4. Efficiency Analysis

#### Computational Efficiency vs. Performance (Table 8)

The experimental results demonstrate that the added algorithmic complexity of eX2L is a necessary investment for superior generalization in difficult settings (full results in Appendix D):

- **Complexity Pay-off:** While most baselines share ERM’s time complexity, they often fail to exceed its performance. In contrast, eX2L-MAE and eX2L-Cosine achieve  $1.20\times$  and  $1.17\times$  better results, respectively, successfully converting additional training time into significant WGA gains.
- **Confounder Precision:** The *Hard Spawrious* performance leap confirms that complex distribution shifts demand the precise confounder treatment eX2L provides.

## 6. Conclusion

We presented eX2L, an explanation-based framework that achieves domain invariance by enforcing spatial disjointness between label and confounder Grad-CAM maps. By providing a transparent mechanism to decouple spurious correlations, eX2L not only mitigates distribution shifts but challenges the perceived trade-off between interpretability and robustness, laying a foundation for algorithmic fairness.

## Impact Statement

This paper presents eX2L, a framework for improving model robustness under distribution shifts via explanation-based regularization. The primary positive societal impact is the potential to reduce model bias in high-stakes deployment settings such as healthcare diagnostics, autonomous systems, and legal analytics, where spurious correlations in training data can lead to discriminatory or unsafe predictions. The interpretable nature of the Grad-CAM penalty also increases the auditability of the debiasing process, which supports accountability in algorithmic decision-making. A potential negative consequence is that practitioners may misapply the framework to settings where confounder labels are unavailable, poorly defined, or themselves biased, which could give false confidence in a model’s robustness. We encourage careful validation of confounder label quality before deploying eX2L in sensitive domains.

## References

- Adebayo, J., Gilmer, J., Muelly, M., Goodfellow, I., Hardt, M., and Kim, B. Sanity checks for saliency maps. In *Proceedings of the 32nd International Conference on Neural Information Processing Systems*, NIPS’18, pp. 9525–9536, Red Hook, NY, USA, 2018. Curran Associates Inc.
- Angarano, S., Martini, M., Salvetti, F., Mazzia, V., and Chiaberge, M. Back-to-bones: Rediscovering the Role of Backbones in Domain Generalization. *Pattern Recognition*, 156:110762, 2024. doi: 10.1016/j.patcog.2024.110762.
- Arjovsky, M., Bottou, L., Gulrajani, I., and Lopez-Paz, D. Invariant risk minimization, 2019. URL <https://arxiv.org/abs/1907.02893>.
- Dammu, P. P. S. and Shah, C. Detecting spurious correlations via robust visual concepts in real and AI-generated image classification. In *XAI in Action: Past, Present, and Future Applications*, 2023. URL <https://openreview.net/forum?id=ewagDhIy8Y>.
- Ganin, Y., Ustinova, E., Ajakan, H., Germain, P., Larochelle, H., Laviolette, F., March, M., and Lempitsky, V. Domain-adversarial training of neural networks. *Journal of machine learning research*, 17(59):1–35, 2016.
- Gretton, A., Borgwardt, K. M., Rasch, M. J., Schölkopf, B., and Smola, A. A kernel two-sample test. *Journal of Machine Learning Research*, 13(25):723–773, 2012. URL <http://jmlr.org/papers/v13/gretton12a.html>.
- Gulrajani, I. and Lopez-Paz, D. In search of lost domain generalization. In *International Conference on Learning Representations*, 2021. URL <https://openreview.net/forum?id=lQdXeXDoWtI>.
- Hagos, M. T., Curran, K. M., and Namee, B. M. Identifying spurious correlations and correcting them with an explanation-based learning, 2022. URL <https://arxiv.org/abs/2211.08285>.
- Han, X. and Tsvetkov, Y. Influence tuning: Demoting spurious correlations via instance attribution and instance-driven updates. In Moens, M.-F., Huang, X., Specia, L., and Yih, S. W.-t. (eds.), *Findings of the Association for Computational Linguistics: EMNLP 2021*, pp. 4398–4409, Punta Cana, Dominican Republic, November 2021. Association for Computational Linguistics. doi: 10.18653/v1/2021.findings-emnlp.374. URL <https://aclanthology.org/2021.findings-emnlp.374/>.
- Kirichenko, P., Izmailov, P., and Wilson, A. G. Last layer re-training is sufficient for robustness to spurious correlations. In *International Conference on Learning Representations*, 2023. URL <https://openreview.net/forum?id=ylpMUNYWpX>.
- Koh, P. W., Sagawa, S., Marklund, H., Xie, S. M., Zhang, M., Balsubramani, A., Hu, W., Yasunaga, M., Phillips, R. L., Gao, I., Lee, T., David, E., Stavness, I., Guo, W., Earnshaw, B. A., Haque, I. S., Beery, S. M., Leskovec, J., Kundaje, A. B., Pierson, E., Levine, S., Finn, C., and Liang, P. Wilds: A benchmark of in-the-wild distribution shifts. In *International Conference on Machine Learning*, 2020. URL <https://api.semanticscholar.org/CorpusID:229156320>.
- Li, H., Pan, S. J., Wang, S., and Kot, A. C. Domain generalization with adversarial feature learning. In *2018 IEEE/CVF Conference on Computer Vision and Pattern Recognition*, pp. 5400–5409, 2018. doi: 10.1109/CVPR.2018.00566.
- Liu, E. Z., Haghgoo, B., Chen, A. S., Raghunathan, A., Koh, P. W., Sagawa, S., Liang, P., and Finn, C. Just train twice: Improving group robustness without training group information. In *Proceedings of the 38th International Conference on Machine Learning*, pp. 6781–6792. PMLR, 2021a.
- Liu, J., Shen, Z., He, Y., Zhang, X., Xu, R., Yu, H., and Cui, P. Towards out-of-distribution generalization: A survey, 2021b. URL <https://arxiv.org/abs/2108.13624>.
- Locatello, F., Bauer, S., Lucic, M., Raetsch, G., Gelly, S., Schölkopf, B., and Bachem, O. Challenging common assumptions in the unsupervised learning of disentangled representations. In *International Conference on Machine Learning*, pp. 4114–4124, 2019.

- Long, M., Cao, Z., Wang, J., and Jordan, M. I. Conditional adversarial domain adaptation. In *Proceedings of the 32nd International Conference on Neural Information Processing Systems, NIPS'18*, pp. 1647–1657, Red Hook, NY, USA, 2018. Curran Associates Inc.
- Lynch, A., Dovonon, G. J.-S., Kaddour, J., and Silva, R. Spawrious: A benchmark for fine control of spurious correlation biases. In *Workshop on Spurious Correlation and Shortcut Learning: Foundations and Solutions*, 2025. URL <https://openreview.net/forum?id=0S0oITNTCz>.
- McInnes, L., Healy, J., and Melville, J. UMAP: Uniform manifold approximation and projection for dimension reduction, 2018. URL <https://arxiv.org/abs/1802.03426>.
- Milletari, F., Navab, N., and Ahmadi, S.-A. V-Net: Fully convolutional neural networks for volumetric medical image segmentation. In *2016 Fourth International Conference on 3D Vision (3DV)*, pp. 565–571, 2016. doi: 10.1109/3DV.2016.79.
- Ming, Y., Yin, H., and Li, Y. On the impact of spurious correlation for out-of-distribution detection. In *Proceedings of the AAAI Conference on Artificial Intelligence*, pp. 10051–10059, 2022. doi: 10.1609/aaai.v36i9.21244.
- Monga, A., Somou, R., Zhang, S., and Ortega, A. Mitigating spurious correlations in image recognition models using performance-based feature sampling. In *Workshop on Spurious Correlation and Shortcut Learning: Foundations and Solutions*, 2025. URL <https://openreview.net/forum?id=DRv8wcsgs>.
- Nam, J., Cha, H., Ahn, S., Lee, J., and Shin, J. Learning from failure: De-biasing Classifier from Biased Classifier. In *Advances in Neural Information Processing Systems*, volume 33, pp. 20673–20684, 2020.
- Rahman, M. A. and Wang, Y. Optimizing intersection-over-union in deep neural networks for image segmentation. In Bebis, G., Boyle, R., Parvin, B., Koracin, D., Porikli, F., Skaff, S., Entezari, A., Min, J., Iwai, D., Sadagic, A., Scheidegger, C., and Isenberg, T. (eds.), *Advances in Visual Computing*, pp. 234–244, Cham, 2016. Springer International Publishing. ISBN 978-3-319-50835-1.
- Sagawa, S., Koh, P. W., Hashimoto, T. B., and Liang, P. Distributionally robust neural networks for group shifts: On the importance of regularization for worst-case generalization, 2019. URL <https://arxiv.org/abs/1911.08731>.
- Sagawa, S., Koh, P. W., Hashimoto, T. B., and Liang, P. Distributionally robust neural networks. In *International Conference on Learning Representations*, 2020. URL <https://openreview.net/forum?id=ryxGuJrFvS>.
- Selvaraju, R. R., Cogswell, M., Das, A., Vedantam, R., Parikh, D., and Batra, D. Grad-cam: Visual explanations from deep networks via gradient-based localization. *International Journal of Computer Vision*, 128 (2):336–359, October 2019. ISSN 1573-1405. doi: 10.1007/s11263-019-01228-7. URL <http://dx.doi.org/10.1007/s11263-019-01228-7>.
- Shen, H. and Zhao, Z. Boosting test performance with importance sampling—a subpopulation perspective. In *Proceedings of the Thirty-Ninth AAAI Conference on Artificial Intelligence and Thirty-Seventh Conference on Innovative Applications of Artificial Intelligence and Fifteenth Symposium on Educational Advances in Artificial Intelligence, AAAI'25/IAAI'25/EAAI'25*. AAAI Press, 2025. ISBN 978-1-57735-897-8. doi: 10.1609/aaai.v39i19.34244. URL <https://doi.org/10.1609/aaai.v39i19.34244>.
- Suhail, P., Goel, V., and Sethi, A. Shortcut learning susceptibility in vision classifiers. In *Workshop on Spurious Correlation and Shortcut Learning: Foundations and Solutions*, 2025. URL <https://openreview.net/forum?id=dvafjL2zXP>.
- Sun, B. and Saenko, K. Deep coral: Correlation alignment for deep domain adaptation. In Hua, G. and Jégou, H. (eds.), *Computer Vision – ECCV 2016 Workshops*, pp. 443–450, Cham, 2016. Springer International Publishing. ISBN 978-3-319-49409-8.
- Tishby, N. and Zaslavsky, N. Deep learning and the information bottleneck principle. In *IEEE Information Theory Workshop*, pp. 1–5, 2015.
- Wang, Z., Bovik, A., Sheikh, H., and Simoncelli, E. Image quality assessment: from error visibility to structural similarity. *IEEE Transactions on Image Processing*, 13 (4):600–612, 2004. doi: 10.1109/TIP.2003.819861.
- Wiles, O., Gowal, S., Stimberg, F., Rebuffi, S.-A., Ktena, I., Dvijotham, K. D., and Cemgil, A. T. A fine-grained analysis on distribution shift. In *International Conference on Learning Representations*, 2022. URL <https://openreview.net/forum?id=D14LetuLdyK>.
- Yang, Y., Zhang, H., Katabi, D., and Ghassemi, M. Change is hard: A closer look at subpopulation shift. In *International Conference on Machine Learning*, 2023.
- Ye, H., Xie, C., Cai, T., Li, R., Li, Z., and Wang, L. Towards a theoretical framework of out-of-distribution generalization. In Ranzato, M., Beygelzimer, A., Dauphin, Y., Liang, P., and Vaughan, J. W. (eds.),

*Advances in Neural Information Processing Systems*,  
volume 34, pp. 23519–23531. Curran Associates, Inc.,  
2021. URL [https://proceedings.neurips.cc/paper\\_files/paper/2021/file/c5c1cb0bebd56ae38817b251ad72bedb-Paper.pdf](https://proceedings.neurips.cc/paper_files/paper/2021/file/c5c1cb0bebd56ae38817b251ad72bedb-Paper.pdf).

## A. Screening Process Results

Table 3. Similarity Function Selection Test Results

Algorithms		Datasets			
Name	Sampling	CMNIST		Waterbirds	
		Train WGA	Val WGA	Train WGA	Val WGA
Cosine	Random	42.51%	8.52%	15.04%	18.05%
<b>Cosine</b>	<b>Uniform Group</b>	72.38%	64.13%	91.55%	<b>85.71%</b>
IoU	Random	5.55%	0.84%	43.48%	44.64%
IoU	Uniform Group	65.67%	65.46%	91.70%	84.55%
JS Dist.	Random	0.00%	0.00%	25.10%	25.70%
<b>JS Dist.</b>	<b>Uniform Group</b>	71.31%	<b>67.83%</b>	88.20%	82.71%
JS Div.	Random	16.02%	8.75%	15.04%	19.55%
JS Div.	Uniform Group	71.19%	66.22%	90.68%	79.70%
KL Div.	Random	10.92%	5.29%	39.13%	45.11%
KL Div.	Uniform Group	68.44%	66.30%	89.41%	82.71%
MAE	Random	4.59%	5.38%	62.50%	53.38%
<b>MAE</b>	<b>Uniform Group</b>	72.20%	66.43%	89.93%	<b>85.71%</b>
MSE	Random	4.90%	2.09%	16.07%	18.05%
MSE	Uniform Group	64.07%	55.15%	87.08%	83.91%
NCC	Random	0.39%	0.30%	17.88%	18.05%
NCC	Uniform Group	72.37%	66.16%	91.60%	82.19%
RMSE	Random	17.74%	2.54%	10.71%	15.79%
RMSE	Uniform Group	65.52%	62.78%	91.09%	84.76%
SSIM	Random	74.77%	22.42%	14.87%	17.99%
<b>SSIM</b>	<b>Uniform Group</b>	71.48%	<b>67.41%</b>	89.97%	81.55%
Soft Dice	Random	15.34%	6.43%	46.43%	40.60%
<b>Soft Dice</b>	<b>Uniform Group</b>	69.79%	<b>66.52%</b>	93.06%	<b>84.96%</b>

As shown in Table 3, algorithms which use Uniform Group Sampling performed better than their Random Sampling counterparts. This can be linked to how Uniform Group Sampling provides balanced views of the dataset per training batch, allowing the algorithm to focus more on decoupling the label and confounder attributes without the added noisiness of random batches.

## B. Additional Methodology Details

### B.1. Acquiring Target Logit in Binary Cases

Given that binary models only provide single logits, to account for the two classes, the following script is used where `target` refers to the actual target variable:

```
target_logit_for_grad = torch.where(targets.bool(), logits, -logits)
```

### B.2. Heatmap Detachment

To avoid the computational costs associated with calculating gradient of gradients, during gradient calculation, `create_graph` is set to `False` to detach the calculation of the heatmap from the backpropagation operation:

```
gradients = torch.autograd.grad(outputs=target_logit_for_grad.sum(),
    inputs=activations['value'],
    retain_graph=True,
    create_graph=False)[0]
```

### B.3. Datasets

**CMNIST** CMNIST is a dataset based on the MNIST dataset, where the labels are divided into "Less than 5", and "Greater than or Equal to 5". (Arjovsky et al., 2019). Arjovsky et al. (2019) adds the spurious correlation, color, by coloring them red or green based on the label. This correlation is subverted at test time, where the spurious correlation is reversed (Arjovsky et al., 2019). Additionally, labels are flipped with a 0.25 probability, to add noise in the dataset (Arjovsky et al., 2019).

**Waterbirds** Waterbirds is a dataset based on the CUB dataset, in which pictures of birds are spuriously correlated with the land or water background (Sagawa et al., 2020). The challenge here is that birds which do not necessarily match with their background (e.g., Water Bird in Land) are minority groups, leading to the problem of subpopulation shift at test time, where they are balanced out again (Sagawa et al., 2020).

**CelebA** CelebA is based on the CelebA celebrity face dataset in which the labels are the hair color, and the confounders are the gender of the image subjects (Sagawa et al., 2020). The spurious correlation here is that most females are blondes, while most males are non-blondes (Sagawa et al., 2020).

**Spawrious** Spawrious is a newer dataset which tests models on unseen domains (mainly dogs and backgrounds), where it has two types and three difficulty (Easy, Medium, Hard) per type (Lynch et al., 2025). One type is "One-to-One" in which dogs are only associated with one background, and this background is changed at test time (Lynch et al., 2025). On the other hand, the "Many-to-Many" creates a many-to-many correlation in which dogs are associated with two backgrounds, and these two backgrounds are changed at test time (Lynch et al., 2025).

Models trained for 300 epochs per dataset, except for *CelebA* which was trained for 50 epochs.

### B.4. Baseline Algorithms

#### B.4.1. EMPIRICAL RISK MINIMIZATION (ERM)

Empirical Risk Minimization (ERM) only follows the standard cross-entropy loss such that in binary-class settings, the binary cross entropy (BCE) loss is used:

$$\text{BCE} = -\frac{1}{n} \sum_{i=1}^n (y_i \cdot \log \hat{y}_i + (1 - y_i) \cdot \log (1 - \hat{y}_i)) \quad (8)$$

For multi-class settings with  $K$  classes, the categorical cross-entropy (CCE) is used:

$$\text{CCE} = -\frac{1}{n} \sum_{i=1}^n \sum_{k=1}^K y_{i,k} \cdot \log \hat{y}_{i,k} \quad (9)$$

where  $y_{i,k} \in \{0, 1\}$  is the indicator that sample  $i$  belongs to class  $k$ .

#### B.4.2. INVARIANT RISK MINIMIZATION (IRM) (ARJOVSKY ET AL., 2019)

Invariant Risk Minimization (IRM) is a learning paradigm developed by Arjovsky et al. (2019) which aims to find invariant, generalizable representations across multiple training environments.

Following Arjovsky et al. (2019), we used IRMv1, its more tractable form for the experiments. Instead of minimizing risk per environment, it minimizes the global environmental risk using a linear invariant predictor:

$$\mathcal{L}_{IRM,w=1.0}(\Phi^\top) = \sum_{e \in \mathcal{E}_{tr}} R^e(\Phi^\top) + \lambda \cdot \mathbb{D}_{lin}(1.0, \Phi^\top, e) \quad (10)$$

where  $w$  is a fixed scalar weight (set to 1.0 in IRMv1),  $\Phi^\top$  serves as the model's parameters,  $R^e$  is the risk for a given environment  $e$  in the set of all training environments  $\mathcal{E}_{tr}$ , and the IRMv1 penalty  $\mathbb{D}_{lin}$  is the squared norm of the normal-equations residual, measuring how far the fixed classifier  $w$  deviates from the environment-optimal linear predictor:

$$\mathbb{D}_{\text{lin}}(w, \Phi, e) = \left\| \mathbb{E}_{X^e} [\Phi(X^e)\Phi(X^e)^\top] w - \mathbb{E}_{X^e, Y^e} [\Phi(X^e)Y^e] \right\|^2 \quad (11)$$

A small value of  $\mathbb{D}_{\text{lin}}(1.0, \Phi, e)$  indicates that  $w=1.0$  is already near-optimal for environment  $e$ , which is the IRMv1 invariance condition.

#### B.4.3. MAXIMUM MEAN DISCREPANCY (MMD) (LI ET AL., 2018)

Li et al. (2018)’s rationale for using MMD regularization is to learn feature representations which would generalize to unseen, non-training domains. By operating on the latent representation of each domain using a mean map operation  $\mu(\cdot)$  to map these representations in the reproducing kernel Hilbert space (RKHS),  $\mathcal{H}$ ,

$$\mu_P := \mu(P) = \mathbb{E}_{x \sim P}[\phi(x)] = \mathbb{E}_{x \sim P}[k(x, \cdot)] \quad (12)$$

where  $\phi: \mathbb{R}^d \rightarrow \mathcal{H}$  is a feature map, and  $k(\cdot, \cdot)$  is the kernel function induced by  $\phi(\cdot)$ . Based on the MMD theory (Li et al., 2018), the distance between the domains  $l$  and  $t$  (or  $\mathbb{P}_l$  and  $\mathbb{P}_t$ ), which serves as the MMD loss, can be measured by:

$$\text{MMD}(\mathbf{H}_l, \mathbf{H}_t) = \|\mu_{\mathbb{P}_l} - \mu_{\mathbb{P}_t}\|_{\mathcal{H}} \quad (13)$$

#### B.4.4. CORRELATION ALIGNMENT (CORAL) (SUN & SAENKO, 2016)

CORAL loss is simply the distance between the covariances  $C$  of the source domain  $S$  and target domain  $T$  features (Sun & Saenko, 2016), as stated by:

$$\mathcal{L}_{\text{CORAL}} = \frac{1}{4d^2} \|C_S - C_T\|_F^2 \quad (14)$$

where  $d$  is the number of input dimensions and  $\|\cdot\|_F^2$  is the squared matrix Frobenius norm. The covariance matrices of the source and target data are given by (Sun & Saenko, 2016):

$$C_S = \frac{1}{n_S - 1} \left( D_S^\top D_S - \frac{1}{n_S} (\mathbf{1}^\top D_S)^\top (\mathbf{1}^\top D_S) \right) \quad (15)$$

$$C_T = \frac{1}{n_T - 1} \left( D_T^\top D_T - \frac{1}{n_T} (\mathbf{1}^\top D_T)^\top (\mathbf{1}^\top D_T) \right) \quad (16)$$

where  $\mathbf{1}$  is a column vector with all elements equal to 1.

#### B.4.5. DOMAIN ADVERSARIAL NEURAL NETWORKS (DANN) (GANIN ET AL., 2016)

In DANN, Ganin et al. (2016) created an adversarial network consisting of a label classifier and a domain classifier, where the novel contribution of the authors is introducing the gradient reversal, in which the additive inverse of the gradient from the domain classifier is backpropagated to the common feature extractor. This leads to the domain classifier being ‘fooled’ by the overall network, while enforcing domain invariance in the label classifier.

This is encapsulated by the objective which penalizes the correct predictions of the domain classifier for each domain, to make the feature extractor’s parameters  $\theta_f$  domain invariant:

$$E(\theta_f, \theta_y, \theta_d) = \frac{1}{n} \sum_{i=1}^n \mathcal{L}_y^i(\theta_f, \theta_y) - \lambda \left( \frac{1}{n} \sum_{i=1}^n \mathcal{L}_d^i(\theta_f, \theta_d) + \frac{1}{n'} \sum_{i=n+1}^N \mathcal{L}_d^i(\theta_f, \theta_d) \right) \quad (17)$$

where  $\theta_d$  and  $\theta_y$  are the parameters of the domain and label classifiers,  $N$  is the total number of data points,  $n'$  is  $N - n$ , and  $\mathcal{L}_d$  and  $\mathcal{L}_y$  are the cross-entropy losses of the label and domain classifiers, respectively.

#### B.4.6. CONDITIONAL DOMAIN ADVERSARIAL NEURAL NETWORKS (CDAN) (LONG ET AL., 2018)

Long et al. (2018) posited that adapting not only the feature extractor, but also the domain classifier on class label information can help in promoting domain invariance. By conditioning the domain classifier on the data point’s class information, the joint distribution of features and class labels across domains can be aligned, without hampering performance by blindly aligning all feature distributions across domains as in DANNs Long et al. (2018).

As compared to DANN whose domain classifier’s function is defined as  $d(f)$  where  $f$  represents the features, CDAN defines its domain classifier function as  $d(f, y)$  where  $(f, y)$  serves as the joint variable for the features and the class information.

#### B.4.7. GROUP DISTRIBUTIONALLY ROBUST OPTIMIZATION (GROUPDRO) (SAGAWA ET AL., 2019)

In GroupDRO (Sagawa et al., 2019), the primary objective is to find the model which minimizes the risk of the worst group, using the intuition that addressing the generalization problem of the worst group would lead to generalizing to other groups.

Sagawa et al. (2019) defines the worst-group risk as:

$$\mathcal{R}(\theta) = \max_{g \in \mathcal{G}} \mathbb{E}_{x,y} P_g[\mathcal{L}(\theta; (x, y))] \quad (18)$$

### B.5. Similarity Functions

#### B.5.1. NEGATIVE MEAN ABSOLUTE ERROR (MAE)

Given that MAE is a distance metric and is boundless, its additive inverse is used to penalize similarity:

$$\text{MAE}_{\text{eX2L}} = -\frac{1}{n} \sum_i |L_i^y - L_i^c| \quad (19)$$

where  $L^y$  and  $L^c$  are Grad-CAM heatmaps of the label and confounder model and  $n$  is the total number of heatmap ‘pixels’.

#### B.5.2. NEGATIVE MEAN SQUARED ERROR (MSE)

Similar to MAE, the additive inverse is also used for MSE:

$$\text{MSE}_{\text{eX2L}} = -\frac{1}{n} \sum_i (L_i^y - L_i^c)^2 \quad (20)$$

#### B.5.3. NEGATIVE ROOT MEAN SQUARED ERROR (RMSE)

Similar to MAE and MSE, the additive inverse is also used for RMSE:

$$\text{RMSE}_{\text{eX2L}} = -\sqrt{\frac{1}{n} \sum_i (L_i^y - L_i^c)^2} \quad (21)$$

#### B.5.4. SOFT INTERSECTION-OVER-UNION (IOU)

Given that the original IoU metric uses non-differentiable operations given that it is defined as the intersection of two sets over their union, we used its approximation as defined by Rahman & Wang (2016):

$$\text{Soft-IoU}_{\text{eX2L}} = \frac{\sum_{i=1}^n L_i^y \cdot L_i^c}{\sum_{i=1}^n (L_i^y + L_i^c - L_i^y \cdot L_i^c)} \quad (22)$$

By penalizing ‘intersections’ in spatial regions, we are then able to penalize confounder reliance in the label model.

### B.5.5. KULLBACK-LEIBLER (KL) DIVERGENCE

The KL Divergence is a non-symmetric metric which measures the difference in information between two distributions. In  $D_{\text{KL}}(P\|Q)$ ,  $P$  is the reference distribution and  $Q$  is the approximating distribution; the divergence is large when  $Q$  is a poor approximation of  $P$ . Here we set the confounder heatmap  $P_{L_{L_1}^c}$  as the reference and the label heatmap  $P_{L_{L_1}^y}$  as the approximating distribution, and use the additive inverse to maximize dissimilarity:

$$D_{\text{KL}}(P_{L_{L_1}^c} \| P_{L_{L_1}^y})_{\text{eX2L}} = \sum_{x \in \mathcal{X}} P_{L_{L_1}^c}(x) \ln \frac{P_{L_{L_1}^c}(x)}{P_{L_{L_1}^y}(x)} \quad (23)$$

where  $P_{L_{L_1}^c}$  refers to the  $L_1$ -normalized probability distribution of the confounder model’s heatmap pixels,  $P_{L_{L_1}^y}$  refers to the  $L_1$ -normalized probability distribution of the label model’s heatmap pixels, and  $\mathcal{X}$  refers to the pixel index space.

This asymmetric choice is deliberate: a large  $D_{\text{KL}}(P_{L_{L_1}^c} \| P_{L_{L_1}^y})$  means the label heatmap is a poor approximation of the confounder heatmap, confirming spatial disjointness. The converse direction, whether the confounder heatmap can approximate the label heatmap, is less informative for our objective because it may simply reflect insufficient training of the confounder model (e.g., under small  $\lambda_c$ ).

### B.5.6. JENSEN-SHANNON (JS) DIVERGENCE

Given KL Divergence’s limitation on having one distribution as a target and another as a source, we also used JS divergence, a symmetric form of the measuring distribution divergences. JS divergence is simply the average of KL divergence of two distributions to the mean of both distributions, where for eX2L, its additive inverse is used (to induce distributional dissimilarity):

$$D_{\text{JS}}(P_{L_{L_1}^c} \| P_{L_{L_1}^y})_{\text{eX2L}} = -\frac{1}{2} D_{\text{KL}} \left( L_{L_1}^c \| \frac{L_{L_1}^c + L_{L_1}^y}{2} \right) - \frac{1}{2} D_{\text{KL}} \left( L_{L_1}^y \| \frac{L_{L_1}^c + L_{L_1}^y}{2} \right) \quad (24)$$

Through this, we are able to simultaneously evaluate the reliance of both models on each other’s supposed conceptual attributes.

### B.5.7. JENSEN-SHANNON DISTANCE (JSD)

While JS Divergence shares some of the same qualities as JS Distance (JSD) such as being bounded and symmetric, JS Divergence does not satisfy the Triangle Inequality, leading to it not being a proper distance metric. Due to being the square root of the JS Divergence, it satisfies the Triangle Inequality, hence serving as a proper distance metric.

Similarly, its additive inverse is used to penalize similarities in distributions of the heatmaps:

$$\text{JSD}_{\text{eX2L}} = -\sqrt{\frac{1}{2} D_{\text{KL}} \left( L_{L_1}^c \| \frac{L_{L_1}^c + L_{L_1}^y}{2} \right) + \frac{1}{2} D_{\text{KL}} \left( L_{L_1}^y \| \frac{L_{L_1}^c + L_{L_1}^y}{2} \right)} \quad (25)$$

### B.5.8. COSINE SIMILARITY

In calculating the Cosine Similarity of the two heatmaps for eX2L, in comparison to the standard Cosine Similarity calculation, the heatmaps are first  $L_1$ -normalized to produce probability distributions from the heatmaps. These  $L_1$ -normalized heatmaps are then flattened to get the cosine similarity between the two heatmaps:

$$\cos(\theta)_{\text{eX2L}} = \frac{\sum_{i=1}^n L_{L_1,i}^c \cdot L_{L_1,i}^y}{\sqrt{\sum_{i=1}^n (L_{L_1,i}^c)^2} \cdot \sqrt{\sum_{i=1}^n (L_{L_1,i}^y)^2}} \quad (26)$$

### B.5.9. NORMALIZED CROSS-CORRELATION (NCC) COEFFICIENT

Given that we do not need the lagging mechanism used in cross-correlation which heavily hinges on identifying similar local features between photos as eX2L aims to compare the same spatial regions, we used its zero-lag form, which can be

simply defined as the Pearson Correlation Coefficient allowing us to compare each heatmap globally:

$$\text{NCC}_{\text{eX2L}} = \frac{\sum_{i=1}^n (L_i^c - \bar{L}^c) \cdot (L_i^y - \bar{L}^y)}{\sqrt{\sum_{i=1}^n (L_i^c - \bar{L}^c)^2} \cdot \sqrt{\sum_{i=1}^n (L_i^y - \bar{L}^y)^2}} \quad (27)$$

where  $\bar{L}^c$  and  $\bar{L}^y$  are the mean of all heatmap pixel values for the confounder and label models, respectively.

#### B.5.10. STRUCTURAL SIMILARITY INDEX MEASURE (SSIM) (WANG ET AL., 2004)

Wang et al. (2004)'s SSIM aims to quantify similarities in structural information using three indicators: luminance; contrast; and structure.

The luminance comparison function is given by the twice the product of the mean pixel intensities ( $\bar{L}^c, \bar{L}^y$ ) of the two heatmaps divided by the sum of their squared mean pixel intensities (Wang et al., 2004). A stabilizing constant  $C_1$  is added to both numerator and denominator to avoid division by zero:

$$l(L^c, L^y) = \frac{2\bar{L}^c \cdot \bar{L}^y + C_1}{(\bar{L}^c)^2 + (\bar{L}^y)^2 + C_1} \quad (28)$$

where  $C_1$  is defined as:

$$C_1 = (K_1 L)^2 \quad (29)$$

where  $K_1 \ll 1$  and  $L$  is the dynamic range of the pixel values (Wang et al., 2004).

The contrast comparison function, on the other hand, is given by:

$$c(L^c, L^y) = \frac{2\sigma_{L^y L^c} + C_2}{\sigma_{L^y}^2 + \sigma_{L^c}^2 + C_2} \quad (30)$$

where  $C_2 = (K_2 L)^2$  and  $K_2 \ll 1$ .

Lastly, the structure comparison function is defined by:

$$s(L^c, L^y) = \frac{\sigma_{L^y L^c} + C_3}{\sigma_{L^y} \sigma_{L^c} + C_3} \quad (31)$$

where  $C_3 = (K_3 L)^2$ ,  $K_3 \ll 1$ . Following Wang et al. (2004), in practice  $C_3 = C_2/2$  (i.e.,  $K_3 = K_2/\sqrt{2}$ ). The sample covariance  $\sigma_{L^y L^c}$  between  $L^y$  and  $L^c$  can be estimated using:

$$\sigma_{L^y L^c} = \frac{1}{n-1} \sum_{i=1}^n (L_i^y - \bar{L}^y)(L_i^c - \bar{L}^c) \quad (32)$$

Altogether, SSIM (Wang et al., 2004) is defined as:

$$\text{SSIM}(L^c, L^y) = [l(L^c, L^y)]^\alpha \cdot [c(L^c, L^y)]^\beta \cdot [s(L^c, L^y)]^\gamma \quad (33)$$

where  $\alpha > 0$ ,  $\beta > 0$ , and  $\gamma > 0$  are parameters used to indicate the relative importance of each comparison function.

B.5.11. SOFT DICE

Given that the original Dice coefficient which is twice the intersection of sets A and B divided by the sum of the cardinality of both sets is not differentiable by itself, we used a non-squared variant of Milletari et al. (2016)’s objective based on the coefficient such that:

$$\text{Soft-Dice}_{\text{eX2L}} = \frac{2 \sum_{i=1}^n L_i^c \cdot L_i^y}{\sum_{i=1}^n (L_i^c) + \sum_{i=1}^n (L_i^y)} \tag{34}$$

Ranging from 0 to 1, through eX2L, this similarity metric penalizes intersection in terms of regions, similar to Soft IoU.

**B.6. Group Proportion Strategy**

For datasets such as *CMNIST* and *Spawrious*, the existing strategy for environment splits designed by (Arjovsky et al., 2019) are used.

In *Waterbirds*, we created group proportions that model differences in environments which would encourage learning of spurious correlation, without proper regularization such that:

Table 4. *Waterbirds* Group Proportions

Environment	Confounder	Label	Proportion	Combined Proportion per Confounder
Land-centric (1)	Land	Waterbird	8.26%	70.06%
Land-centric (1)	Land	Landbird	61.80%	
Land-centric (1)	Water	Waterbird	11.58%	29.95%
Land-centric (1)	Water	Landbird	18.37%	
Balanced (2)	Land	Waterbird	5.98%	50.75%
Balanced (2)	Land	Landbird	44.77%	
Balanced (2)	Water	Waterbird	19.05%	49.25%
Balanced (2)	Water	Landbird	30.20%	

Each environment is made more distinct in terms of group proportions to ensure that the domain generalization algorithms learn different shifts in subpopulations.

In *CelebA*, we created group proportions that model differences in sex, to encourage the unregularized model to learn the spurious correlation of sex, with the primary attribute, hair color:

Table 5. *CelebA* Group Proportions

Environment	Confounder	Label	Proportion	Combined Proportion per Confounder
Balanced (1)	Male	Blonde	1.08%	48.02%
Balanced (1)	Male	Non-Blonde	46.94%	
Balanced (1)	Female	Blonde	10.20%	51.97%
Balanced (1)	Female	Non-Blonde	41.77%	
Less Males (2)	Male	Blonde	0.66%	35.85%
Less Males (2)	Male	Non-Blonde	35.19%	
Less Males (2)	Female	Blonde	17.36%	64.15%
Less Males (2)	Female	Non-Blonde	46.79%	

Again, each environment is made more balanced or imbalanced to ensure that the domain generalization algorithms learn different shifts in subpopulations.

### B.7. Initial Grid Search Parameters

The values used for conducting the initial grid search are 0.001, 0.01, 0, 1, 10, 100 for both  $\lambda_y$  and  $\lambda_c$ . Based on the initial results from the grid search on *CMNIST* and *Waterbirds*, the performance is most optimal between 0.1 and 100, leading to the hyperparameter uniform distribution,  $U(0.1, 100)$  for both  $\lambda_y$  and  $\lambda_c$ .

### B.8. Hyperparameter Grid (Gulrajani & Lopez-Paz, 2021)

To promote better comparability, the hyperparameters used for doing the randomized search are based on the following random distribution used by Gulrajani & Lopez-Paz (2021) in their DomainBed evaluation. Their table is rectified to follow the current iteration of their hyperparameter registry and what was done in the eX2L experiments, as shown in Table 6:

Table 6. Hyperparameter Search Space and Default Values

Condition	Parameter	Default Value	Random Distribution
ResNet	Batch size	128	—
MNIST	Learning rate	0.00005	$10^{\text{Uniform}(-5, -3.5)}$
	Label model learning rate	0.00005	$10^{\text{Uniform}(-5, -3.5)}$
	Confounder model learning rate	0.00005	$10^{\text{Uniform}(-5, -3.5)}$
	Gen. learning rate	0.00005	$10^{\text{Uniform}(-5, -3.5)}$
	Disc. learning rate	0.00005	$10^{\text{Uniform}(-5, -3.5)}$
	Weight decay	0	0
	Gen. weight decay	0	0
Not MNIST	Learning rate	0.001	$10^{\text{Uniform}(-4.5, -3.5)}$
	Label model learning rate	0.001	$10^{\text{Uniform}(-4.5, -2.5)}$
	Confounder model learning rate	0.001	$10^{\text{Uniform}(-4.5, -2.5)}$
	Gen. learning rate	0.001	$10^{\text{Uniform}(-4.5, -2.5)}$
	Disc. learning rate	0.001	$10^{\text{Uniform}(-4.5, -2.5)}$
	Weight decay	0	$10^{\text{Uniform}(-6, -2)}$
	Gen. weight decay	0	$10^{\text{Uniform}(-6, -2)}$
eX2L	Lambda ( $y$ )	1.0	$10^{\text{Uniform}(-1, 2)}$
	Lambda ( $c$ )	1.0	$10^{\text{Uniform}(-1, 2)}$
	Label model weight decay	0	$10^{\text{Uniform}(-6, -2)}$
	Confounder model weight decay	0	$10^{\text{Uniform}(-6, -2)}$
DANN, C-DANN	Lambda	1.0	$10^{\text{Uniform}(-2, 2)}$
	Disc. weight decay	0	$10^{\text{Uniform}(-6, -2)}$
	Disc. steps	1	$2^{\text{Uniform}(0, 3)}$
IRM	Gradient penalty	0	$10^{\text{Uniform}(-2, 1)}$
	Lambda	100	$10^{\text{Uniform}(-1, 5)}$
GroupDRO	Penalty annealing iters.	500	$10^{\text{Uniform}(0, 4)}$
	Eta	0.01	$10^{\text{Uniform}(-1, 1)}$
MMD	Gamma	1	$10^{\text{Uniform}(-1, 1)}$

### B.9. Reproducibility

Experiments were conducted using PyTorch 2.10 and CUDA 12.1 on NVIDIA A100 and L4 GPUs. We enforced deterministic CUDNN and Torch settings to ensure comparative validity.

The following script is used to ensure reproducibility, which also considers the usage of workers:

```
os.environ["CUBLAS_WORKSPACE_CONFIG"] = ":4096:8"

def set_seed(seed):
    random.seed(seed)
    np.random.seed(seed)
    torch.manual_seed(seed)
```

```

torch.cuda.manual_seed(seed)
torch.cuda.manual_seed_all(seed)
torch.backends.cudnn.deterministic = True
torch.backends.cudnn.benchmark = False
torch.use_deterministic_algorithms(True)
os.environ['PYTHONHASHSEED'] = str(seed)

def seed_worker(worker_id):
    worker_seed = torch.initial_seed() % 2**32
    np.random.seed(worker_seed)
    random.seed(worker_seed)

set_seed(seed)
g = torch.Generator()
g.manual_seed(seed)

dataloader = DataLoader(dataset, batch_size=batch_size, shuffle=True,
    pin_memory=True, num_workers=num_workers,
    persistent_workers=True, worker_init_fn=seed_worker,
    prefetch_factor=2, generator=g,
)

```

## B.10. Choice of Explanation Method

eX2L uses Grad-CAM (Selvaraju et al., 2019) as the explanation signal during training rather than input-gradient methods such as Integrated Gradients or SHAP. The key distinction, established by Adebayo et al. (2018), is that many input-gradient methods produce explanations that remain invariant under network reparametrization: they function effectively as unsupervised edge detectors whose output reflects image structure more than learned model behavior. Grad-CAM, by contrast, is sensitive to the current parameter state of the network, making its output a faithful reflection of *what the model has specifically learned to attend to* at each training step. This parameter-sensitivity is essential for eX2L: the  $\mathcal{L}_{\text{sim}}$  penalty is designed to penalize overlap between model-specific visual attention patterns, not between shared structural features of the input image. Using an input-agnostic method would therefore conflate learned attention with image edges, undermining the debiasing signal. Extension to other parameter-sensitive attribution methods (e.g., GradCAM++ or Score-CAM) is a natural future direction and would not require architectural changes to eX2L.

## C. CelebA Results

On *CelebA*, eX2L performs comparably to GroupDRO, the leading algorithm on this benchmark. The results reveal an important insight about the relationship between confounder geometry and similarity metric selection.

**Why hair color is a harder confounder.** Background confounders (e.g., land/water in Waterbirds, breed-background pairs in Spawrious) produce spatially tight, high-contrast heatmap regions that are easily distinguished from label-relevant features. Hair color, by contrast, occupies diffuse, low-contrast areas of the face image that often overlap with structurally important regions (e.g., the top of the head, which is also part of the subject’s identity). This means the label model and confounder model will inevitably share some activated pixels in the CelebA setting, not because of spurious learning, but because both the label (hair color) and the confounder (gender) involve the same physical region.

**Effect on similarity metrics.** Strict pixel-wise penalties such as MAE apply uniform pressure across all pixels, overpenalizing semantically valid co-activations where the label feature and confounder feature genuinely co-occur in space. Softer similarity metrics (Cosine, Soft Dice) are more tolerant of partial overlap and better suited to this geometry. This explains the pattern in Table 7: eX2L-Cosine and eX2L-Soft Dice match GroupDRO’s WGA (84.07%) while maintaining competitive AA (91.19% and 91.70%), whereas eX2L-MAE underperforms in this setting.

**Implications.** CelebA does not indicate a failure of the eX2L framework; it indicates that metric selection should be informed by confounder geometry. The ablation in Appendix A confirms this: metrics that perform best on background confounders (MAE) are not universally optimal, and practitioners should use the screening protocol to select the appropriate similarity function for their confounder type.

Table 7. CelebA Experiment Results

Algorithms		Subpopulation Shift	
Name	Sampling	CelebA	
		AA	WGA
<i>Baselines</i>			
ERM	Random	95.56 $\pm$ 0.0%	39.63 $\pm$ 2.6%
IRM	Uniform Env.	91.17 $\pm$ 0.0%	82.04 $\pm$ 1.8%
MMD	Uniform Env.	92.19 $\pm$ 0.3%	81.30 $\pm$ 1.4%
CORAL	Uniform Env.	92.20 $\pm$ 0.4%	82.41 $\pm$ 0.8%
DANN	Uniform Env.	92.23 $\pm$ 0.3%	80.93 $\pm$ 2.2%
CDAN	Uniform Env.	90.16 $\pm$ 0.2%	80.56 $\pm$ 2.2%
<b>GroupDRO</b>	<b>Uniform Group</b>	<b>91.94 <math>\pm</math>0.3%</b>	<b>84.07 <math>\pm</math>0.6%</b>
<i>Ours</i>			
eX2L-MAE	Uniform Group	90.79 $\pm$ 0.2%	82.59 $\pm$ 2.0%
<b>eX2L-Cosine</b>	<b>Uniform Group</b>	<b>91.19 <math>\pm</math>0.3%</b>	<b>84.07 <math>\pm</math>1.6%</b>
<b>eX2L-Soft Dice</b>	<b>Uniform Group</b>	<b>91.70 <math>\pm</math>0.3%</b>	<b>83.33 <math>\pm</math>1.0%</b>
eX2L-JS Dist.	Uniform Group	90.05 $\pm$ 0.5%	84.07 $\pm$ 1.7%
eX2L-SSIM	Uniform Group	91.39 $\pm$ 0.2%	80.93 $\pm$ 2.7%

## D. Other Efficiency Analysis Results

As seen in most tables, eX2L exhibits a time-performance trade-off, where the added time complexity provides a corresponding increase in performance relative to the baseline ERM.

Table 8. Time-Performance Trade-off in *Hard Many-to-Many Spawrious* Benchmark

Algorithms	time <sub>epoch</sub> (s)	WGA	$\frac{\text{time}_{\text{epoch}}}{\text{time}_{\text{epoch}}^{\text{ERM}}}$	$\frac{\text{WGA}}{\text{WGA}^{\text{ERM}}}$
<i>Baselines</i>				
ERM	207.45	54.91	—	—
IRM	207.28	35.19	1.00 $\times$	0.64 $\times$
MMD	207.71	54.35	1.00 $\times$	0.99 $\times$
CORAL	208.61	53.74	1.01 $\times$	0.98 $\times$
DANN	204.95	55.41	0.99 $\times$	1.01 $\times$
CDAN	209.49	48.23	1.01 $\times$	0.88 $\times$
GroupDRO	213.01	54.40	1.03 $\times$	0.99 $\times$
<i>Ours</i>				
<b>eX2L-MAE</b>	403.50	<b>66.31</b>	1.95 $\times$	<b>1.21<math>\times</math></b>
<b>eX2L-Cosine</b>	403.76	<b>64.25</b>	1.95 $\times$	<b>1.17<math>\times</math></b>
eX2L-Soft Dice	405.98	54.09	1.96 $\times$	0.99 $\times$
eX2L-JS Dist.	415.73	38.02	2.00 $\times$	0.69 $\times$
eX2L-SSIM	406.36	46.10	1.96 $\times$	0.84 $\times$

## E. Architecture Generalization Analysis

To evaluate whether eX2L’s gains are tied to a specific backbone, we compared eX2L against ERM and GroupDRO on the *Hard Many-to-Many Spawrious* benchmark using two additional architectures: a legacy backbone (AlexNet) and a modern high-capacity backbone (ConvNeXt-Base). All results use the best eX2L variant (MAE) and Uniform Group Sampling for eX2L and GroupDRO.

**Architectural Bottleneck.** In the AlexNet regime, all algorithms converge to a near-zero WGA floor. This suggests the bottleneck is the backbone’s representational capacity rather than the optimization strategy; the marginal differences are statistically negligible because AlexNet cannot encode group-invariant features effectively.

Table 9. Time-Performance Trade-off in *CMNIST* Benchmark

Algorithms	time <sub>epoch</sub> (s)	WGA	$\frac{\text{time}_{\text{epoch}}}{\text{time}_{\text{epoch}}^{\text{ERM}}}$	$\frac{\text{WGA}}{\text{WGA}_{\text{ERM}}}$
<i>Baselines</i>				
ERM	47.42	25.11	—	—
IRM	47.43	64.59	1.00×	2.57×
MMD	47.56	61.98	1.00×	2.47×
CORAL	47.49	59.23	1.00×	2.36×
DANN	46.19	66.42	0.97×	2.65×
CDANN	47.05	21.00	0.99×	0.84×
GroupDRO	49.66	63.79	1.05×	2.54×
<i>Ours</i>				
<b>eX2L-MAE</b>	93.28	<b>67.63</b>	1.97×	<b>2.69×</b>
eX2L-JS Dist.	93.36	66.88	1.97×	2.66×
eX2L-Cosine	93.96	66.15	1.98×	2.63×
eX2L-SSIM	95.67	65.87	2.02×	2.62×
eX2L-Soft Dice	93.33	65.14	1.97×	2.59×

Table 10. Time-Performance Trade-off in *Waterbirds* Benchmark

Algorithms	time <sub>epoch</sub> (s)	WGA	$\frac{\text{time}_{\text{epoch}}}{\text{time}_{\text{epoch}}^{\text{ERM}}}$	$\frac{\text{WGA}}{\text{WGA}_{\text{ERM}}}$
<i>Baselines</i>				
ERM	14.05	23.68	—	—
IRM	13.58	84.42	0.97×	3.57×
MMD	13.91	85.64	0.99×	3.62×
CORAL	13.69	85.41	0.97×	3.61×
DANN	13.69	85.41	0.97×	3.61×
CDANN	13.61	84.71	0.97×	3.58×
GroupDRO	14.34	85.95	1.02×	3.63×
<i>Ours</i>				
<b>eX2L-MAE</b>	28.45	<b>87.45</b>	2.02×	<b>3.69×</b>
eX2L-Soft Dice	28.54	86.92	2.03×	3.67×
eX2L-Cosine	28.68	85.72	2.04×	3.62×
eX2L-JS Dist.	27.70	85.10	1.97×	3.59×
eX2L-SSIM	28.79	85.10	2.05×	3.59×

**Explanation Fidelity and Scaling.** With ConvNeXt-Base, eX2L substantially outperforms both ERM and GroupDRO (+15.99% WGA over ERM; +2.78% WGA over GroupDRO). This demonstrates that eX2L’s efficacy is tied to the backbone’s ability to produce spatially precise Grad-CAM maps. AlexNet’s limited receptive field yields noisy, low-resolution heatmaps that undermine the similarity penalty, while ConvNeXt-Base provides the spatial granularity required to discriminate spurious from invariant regions. These results corroborate observations by [Angarano et al. \(2024\)](#) on the positive relationship between backbone capacity and domain generalization performance, and further show that eX2L exhibits superior scaling properties relative to ERM and GroupDRO, extracting greater gains from increased backbone capacity. The ResNet-50 results in the main paper thus evaluate eX2L at its high-capacity ceiling rather than its representational floor.

## F. Limitations and Future Work

**Confounder Label Dependency.** eX2L requires image-level confounder annotations at training time to supervise the auxiliary confounder classifier. This assumption is justified in high-stakes deployment settings such as medical imaging, autonomous driving, and algorithmic fairness auditing, where identifying confounders is already a regulatory or operational necessity, and the costs of annotation are outweighed by the risks of a biased model. Nevertheless, this requirement limits applicability in exploratory settings where nuisance attributes are unknown or costly to label. A natural extension is to replace the supervised confounder classifier with an unsupervised or self-supervised confounder discovery mechanism (e.g., clustering-based approaches, or the signal-detection framework of [Dammu & Shah \(2023\)](#)), enabling annotation-free debiasing. We leave this as an important direction for future work.

Table 11. Time-Performance Trade-off in *Celeba* Benchmark

Algorithms	$\text{time}_{\text{epoch}}(\text{s})$	WGA	$\frac{\text{time}_{\text{epoch}}}{\text{time}_{\text{epoch}}^{\text{ERM}}}$	$\frac{\text{WGA}}{\text{WGA}_{\text{ERM}}}$
<i>Baselines</i>				
ERM	207.39	39.63	—	—
IRM	208.03	82.04	1.00×	2.07×
MMD	208.47	81.30	1.01×	2.05×
CORAL	208.53	82.41	1.01×	2.08×
DANN	205.12	80.93	0.99×	2.04×
CDANN	207.66	80.56	1.00×	2.03×
GroupDRO	213.10	84.07	1.03×	2.12×
<i>Ours</i>				
<b>eX2L-Cosine</b>	403.76	<b>84.07</b>	1.95×	<b>2.12×</b>
<b>eX2L-JS Dist.</b>	406.36	<b>84.07</b>	1.96×	<b>2.12×</b>
eX2L-Soft Dice	405.98	83.33	1.96×	2.10×
eX2L-MAE	403.50	82.59	1.95×	2.08×
eX2L-SSIM	415.73	80.93	2.00×	2.04×

Table 12. Time-Performance Trade-off in *Easy One-to-One Spawrious* Benchmark

Algorithms	$\text{time}_{\text{epoch}}(\text{s})$	WGA	$\frac{\text{time}_{\text{epoch}}}{\text{time}_{\text{epoch}}^{\text{ERM}}}$	$\frac{\text{WGA}}{\text{WGA}_{\text{ERM}}}$
<i>Baselines</i>				
ERM	26.58	84.12	—	—
IRM	26.87	86.20	1.01×	1.02×
MMD	26.97	86.17	1.01×	1.02×
CORAL	27.00	86.43	1.02×	1.03×
DANN	26.49	87.55	1.00×	1.04×
CDANN	26.61	85.24	1.00×	1.01×
GroupDRO	28.23	90.32	1.06×	1.07×
<i>Ours</i>				
<b>eX2L-MAE</b>	52.16	<b>88.05</b>	1.96×	<b>1.05×</b>
eX2L-JS Dist.	52.16	87.74	1.96×	1.04×
eX2L-Cosine	52.12	87.71	1.96×	1.04×
eX2L-SSIM	52.80	85.96	1.99×	1.02×
eX2L-Soft Dice	52.11	81.78	1.96×	0.97×

**Scope and Generality.** eX2L was primarily evaluated on binary image classification benchmarks with known spurious backgrounds or attribute confounders. While the Spawrious Many-to-Many Hard results demonstrate robustness to compositional, multi-environment shifts, extension to multi-label classification, non-image modalities, and transformer-based architectures (e.g., Vision Transformers) remains an open research question. The architecture generalization analysis in Appendix E shows that eX2L’s efficacy scales with backbone capacity, suggesting that higher-fidelity explanations available in modern architectures may further amplify performance gains. Extension to NLP settings (e.g., penalizing overlap between token attribution maps for class and confounder classifiers) is a promising direction given the widespread use of Grad-CAM analogues in transformer attention.

**Comparison with Model-Debiasing Methods.** eX2L is designed as a single-stage loss-based regularizer and was benchmarked against methods of the same class (ERM, IRM, CORAL, DANN, GroupDRO) following the WILDS and DomainBed evaluation protocols (Koh et al., 2020; Gulrajani & Lopez-Paz, 2021). Two-stage model-debiasing methods such as Just Train Twice (JTT) (Liu et al., 2021a), Deep Feature Reweighting (DFR) (Kirichenko et al., 2023), and Learning from Failure (LFF) (Nam et al., 2020), operate under different assumptions (they discover spurious correlations implicitly from failure patterns on a biased model and then fine-tune) and require a separate reweighting or fine-tuning stage, making direct side-by-side comparison in a single-training-run protocol non-trivial. A unified benchmark comparing single-stage regularizers with two-stage debiasing methods under identical group annotation budgets would be a valuable contribution to the community and is a direction we encourage in future work.

Table 13. Performance on AlexNet (Constrained) on *Hard M2M Spawrious*

Algorithm	WGA	AA
eX2L-MAE	3.17%	28.25%
ERM	3.82%	28.20%
GroupDRO	2.84%	28.05%

Table 14. Performance on ConvNeXt-Base (High-Capacity) on *Hard M2M Spawrious*

Algorithm	WGA	AA
<b>eX2L-MAE</b>	<b>50.44%</b>	<b>73.41%</b>
ERM	34.44%	62.61%
GroupDRO	47.66%	71.01%

**Computational Overhead.** Computing Grad-CAM heatmaps during training approximately doubles wall-clock time relative to ERM (see Appendix D). For very large-scale datasets or high-resolution inputs, this overhead may be prohibitive. Potential mitigations include gradient checkpointing, approximating Grad-CAM with cached activations, or using lighter attribution variants (e.g., GradCAM++) as drop-in replacements. The time-performance trade-off demonstrated across all benchmarks indicates that this cost is justified in difficult distribution shift settings where baseline methods fail.